

Photoactivatable Fluorogens by Intramolecular C-H Insertion of Perfluoroaryl Azide

Sheng Xie, Giampiero Proietti, Olof Ramstrom, and Mingdi Yan

J. Org. Chem., **Just Accepted Manuscript** • DOI: 10.1021/acs.joc.9b02050 • Publication Date (Web): 07 Oct 2019

Downloaded from pubs.acs.org on October 7, 2019

Just Accepted

“Just Accepted” manuscripts have been peer-reviewed and accepted for publication. They are posted online prior to technical editing, formatting for publication and author proofing. The American Chemical Society provides “Just Accepted” as a service to the research community to expedite the dissemination of scientific material as soon as possible after acceptance. “Just Accepted” manuscripts appear in full in PDF format accompanied by an HTML abstract. “Just Accepted” manuscripts have been fully peer reviewed, but should not be considered the official version of record. They are citable by the Digital Object Identifier (DOI®). “Just Accepted” is an optional service offered to authors. Therefore, the “Just Accepted” Web site may not include all articles that will be published in the journal. After a manuscript is technically edited and formatted, it will be removed from the “Just Accepted” Web site and published as an ASAP article. Note that technical editing may introduce minor changes to the manuscript text and/or graphics which could affect content, and all legal disclaimers and ethical guidelines that apply to the journal pertain. ACS cannot be held responsible for errors or consequences arising from the use of information contained in these “Just Accepted” manuscripts.

Photoactivatable Fluorogens by Intramolecular C-H Insertion of Perfluoroaryl Azide

Sheng Xie,^{*,†,‡} Giampiero Proietti,[‡] Olof Ramström,^{*,‡,§,⊥} and Mingdi Yan^{*,§}

[†]State Key Laboratory of Chemo/Biosensing and Chemometrics, College of Chemistry and Chemical Engineering, Hunan University, Changsha 410082, P. R. China; [‡]Department of Chemistry, KTH - Royal Institute of Technology, Teknikringen 36, SE-100 44 Stockholm, Sweden; [§]Department of Chemistry, University of Massachusetts Lowell, Lowell, MA 01854, USA; [⊥]Department of Chemistry and Biomedical Sciences, Linnaeus University, SE-39182 Kalmar, Sweden.

*E-mail: shengxie@hnu.edu.cn, olof_ramstrom@uml.edu, mingdi_yan@uml.edu

ABSTRACT: Molecules capable of fluorescence turn-on by light are highly sought-after in spatio-temporal labeling, surface patterning, monitoring cellular and molecular events, and high-resolution fluorescence imaging. In this work, we report a fluorescence turn-on system based on photo-initiated intramolecular insertion of azide into the neighboring aromatic ring. The azide-masked fluorogens were efficiently synthesized via a cascade nucleophilic aromatic substitution of perfluoroaryl azides with carbazoles. The scaffold also allows for derivatization with biological ligands, as exemplified with D-mannose in this study. This photo-initiated intramolecular transformation led to high yields, high photo-conversion efficiency, and well-separated wavelengths for photo-activation and fluorescence excitation. The mannose-derivatized structure enabled spatio-temporal activation, and showed high contrast and signal amplification. Live cell imaging suggested that the mannose-tagged fluorogen was transported to the lysosomes.

INTRODUCTION

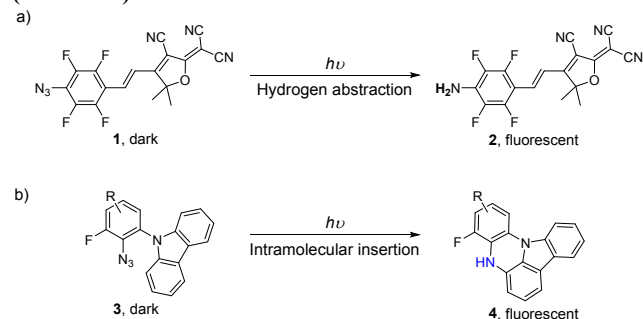
Fluorescence imaging has become an essential tool to study biological events both *in vitro* and *in vivo*. Photoactivatable fluorogens, molecules that become fluorescent upon light irradiation, enable turn-on fluorescence as well as spatial and temporal control, and have thus emerged as an important class of fluorophores finding unique applications in surface patterning, *in situ* labeling,^{1,2} tracking cells and macromolecules,³ and high resolution fluorescence imaging such as PALM (photo-activated localization microscopy).⁴⁻⁷ In these applications, as the photo-controllable fluorogenic transformation dictates the quality of the imaging, it is important that the photochemical reaction is robust and yields clean transformations.⁴ For practical reasons, other requirements are also necessary for these fluorogens, including modular synthesis, straightforward ligand functionalization, biocompatibility with minimum perturbation of the biological system, high signal-to-noise ratio, high photo-stability, minimal susceptibility to environmental changes, specific labeling ability, and good compatibility with microscopy techniques (especially confocal laser microscopy).⁸ In cell imaging, light-controlled fluorescent proteins are highly popular, but suffer from limited spectral variation, photo-bleaching, and environmental sensitivity.⁹ In this regard, small organic photo-activatable compounds have become an increasingly important class of fluorogens,¹⁰ including caged dyes,^{11,12} photo-activated and fluorogenic reaction-based platforms (*e.g.*, those accomplished by the tetrazole-alkene cycloaddition reaction,¹³ photocyclodehydrogenation,^{2,14,15} photo-oxidative dehydrogenation,¹⁶ azide-to-amine photo-reduction,¹⁷⁻²¹ and reversible isomerization²²). In these systems, a photo-sensitive group is used to mask the fluorescence of the fluorogen, for on-demand removal or transformation by a photo-controlled reaction to generate the fluorophore. These reaction-based

designs are mostly modular and can be readily tailored for different applications.

One such photo-sensitive group to mask fluorophores in the dark state is the azide. In this case, the fluorescence can be switched on upon transformation of the azide, for example, by H₂S reduction,²³ photo-reduction,¹⁷⁻²¹ or ‘click’ conjugation.²⁴ In particular, the photochemical azide (1)-to-amine (2) conversion has been demonstrated to be a successful strategy in PALM by Moerner and coworkers (Scheme 1a).¹⁷⁻²¹ The photochemical azide-to-amine reduction reaction is mediated by the aryl nitrene after extrusion of nitrogen, which then undergoes hydrogen abstraction.^{25,26} This high spatial resolution was attributed to an efficient azide-to-amine transformation (87%) in the film, and thus higher signal-to-noise compared to non-fluorinated aryl azide derivatives.²¹ A potential issue with this protocol is the random insertion of the fluorinated nitrene into nearby molecular structures, as for example used in fluorogenic photo-affinity labeling.²¹ This could cause high background noise and also result in potential perturbation of the biosystem.²¹ Additionally, it is not trivial to introduce functional groups on these molecules for subsequent conjugation.

Nitrenes generated by thermolysis or photolysis of azides can also react with neighboring C-H bonds to form *N*-heterocycles, for example, in the synthesis of carbazoles.^{27,28} Consistent with the studies of many non-fluorinated aryl azides, nitrenes generated in these cases also led to a range of other products, for example, those via ring rearrangement pathways.²⁹ It has been extensively studied and shown that the introduction of fluorine atoms *ortho* to the aryl azide increases the lifetime and inhibits ring-expansion rearrangement of the photo-generated singlet nitrenes, leading to higher yields of the C-H and N-H insertion products compared to the non-fluorinated aryl azide analogs.²⁹ We have developed a series of perfluoroaryl azides

Scheme 1. Photo-activatable PFAA fluorogens via a) hydrogen abstraction,¹⁷⁻²¹ and b) intramolecular insertion (this work).



(PFAAs) as a general class of heterobifunctional coupling reagents to immobilize molecules onto surfaces and nanomaterials by photocoupling.^{30,31} Herein, we demonstrate a new fluorescence turn-on strategy based on the intramolecular C-H insertion of perfluoroaryl nitrenes into neighboring aromatic rings (Scheme 1b). While the PFAAs (**3**) are non-fluorescent, the fluorescence can be turned on by photochemical conversion to the corresponding fluorescent carbazole structure (**4**). The reaction is efficient and modular, where additional molecules can be conjugated through

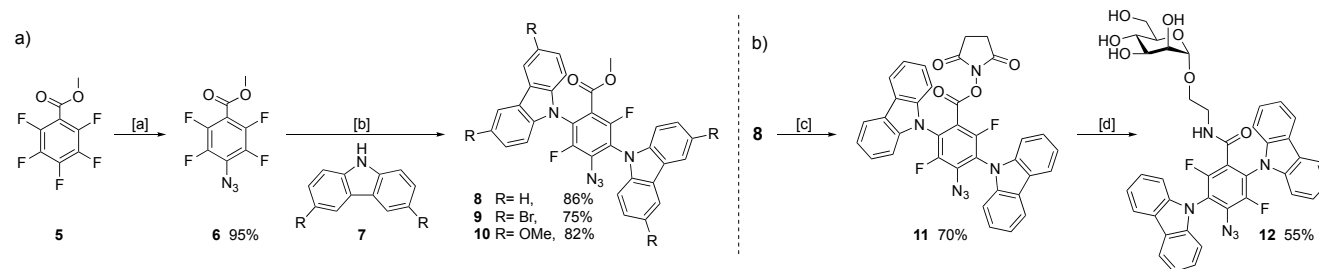
functional groups (R) on the PFAAs. As an example, a carbohydrate, D-mannose, was introduced onto the fluorogen and was used to evaluate the performance of this conjugate in cell imaging.

RESULTS AND DISCUSSION

Synthesis of PFAA fluorogens

The photoactivatable PFAA fluorogens were synthesized following a straightforward protocol via nucleophilic aromatic substitution in two steps from the commercially available starting material methyl pentafluorobenzoate **5** (Scheme 2).⁴⁴ Refluxing **5** and sodium azide in acetone/water afforded PFAA **6** in 95% yield. When PFAA **6** and carbazole **7** were mixed in DMSO in the presence of Cs₂CO₃ at 50 °C for 8 h, di-substituted aryl azides were formed exclusively in high isolated yields (products **8**, 86%; **9**, 75%; **10**, 82%). The conversion was much slower when other solvents such as DMF, MeCN or THF were used (Table 1). This is likely due to the excellent solvation ability of DMSO for the Cs⁺ cation, which is known to enhance the basicity of cesium salts.³² Other bases were also tested (Table 1). For weaker bases like K₂CO₃, longer reaction time (24 h) was needed and the yield (75%) was lower than with Cs₂CO₃. In the case of NEt₃, complete transformation of the

Scheme 2. Synthesis of (a) PFAA fluorogens 8-10, and (b) mannose-derivatized PFAA fluorogen 12.



Conditions: [a] compound **5** (40 mmol), NaN₃ (52 mmol), acetone/water 2:1 (90 mL), reflux, 6 h; [b] compound **6** (0.4 mmol), compound **7** (1.1 mmol), Cs₂CO₃ (2.0 mmol), DMSO (5 mL), 50 °C, 8 h; [c] i. NaOH, MeOH, r.t., 5 h; ii. NHS, EDAC, DCM, 40 °C, 48 h. [d] 2-aminoethyl α -D-mannopyranoside, DMF, in dark, r.t., 24 h.

Table 1. Optimization of reaction conditions.

entry	base	solvent	time/temp.	8 (%) ^b	8:8a ^b
1	Cs ₂ CO ₃	DMSO	12 h / 25 °C	97 (86 ^c)	n.d.
2	Cs ₂ CO ₃	DMF	12 h / 25 °C	76	n.d.
3	Cs ₂ CO ₃	MeCN ^a	12 h / reflux	44	14:1
4	Cs ₂ CO ₃	THF	24 h / reflux	37	8:1
5	NEt ₃	DMSO	72 h / 80 °C	17	3:1
6	K ₂ CO ₃	DMSO	24 h / 25 °C	75	n.d.
7	NaH ^e	DMSO	12 h / 25 °C	53	- ^d
8	<i>t</i> -BuOK ^e	DMSO	12 h / 25 °C	68 (52 ^e)	- ^d
9	<i>t</i> -BuOK ^e	MeCN ^a	3 h / 25 °C	16	7:1

Conditions: PFAA **6** (0.4 mmol, 1 equiv.), carbazole **7a** (0.8 mmol), base (1.0 mmol), solvent (5 mL). ^aSolvent (20 mL). ^bDetermined by ¹⁹F-NMR. ^cIsolated yield. ^dCompound **8a** not detected. ^eBase (0.4 mmol). n.d., compound **8a** not determined.

azide could not be accomplished even at higher temperature, and the reaction time needed to be substantially extended (17% yield at 80 °C after 72 h). Stronger bases, such as NaOH and *t*-BuOK, gave faster conversions but lower isolated product yields. In these cases, significant amounts of dark-colored by-products containing the carbazole moiety were observed, together with the corresponding aniline from PFAA **6**.

The reaction occurs through two sequential substitutions of the aromatic fluorine by the carbazole nitranion. Interestingly, the mono-substituted product **8a** was detected only in trace amount (Table 1), even when a large excess of PFAA **6** (8 eq.) was used.³³ In the mono-substituted product, the large planar carbazole group is expected to be nearly perpendicular to the aryl ring due to steric repulsion. This strongly decreases the conjugative donation of the non-bonding electrons on nitrogen.³⁴ As a result, the carbazole moiety activates the C-F bond in the *para*-position. This *para*-favored double substitution pattern is frequently observed in the nucleophilic aromatic substitution of polyfluoroaromatics.^{35,36}

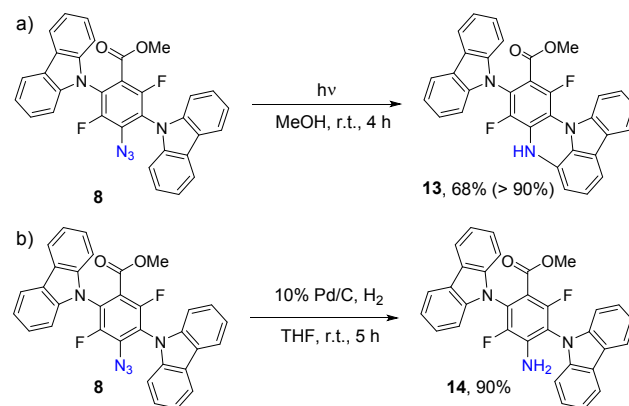
The carboxyl group on the PFAA fluorogen can be further modified, thus allowing convenient incorporation of this photoactivatable fluorogen into other molecules and materials.³⁰ Here, we installed an α -D-mannopyranosyl (Man) group on compound **8** by first converting the methyl ester to an activated NHS ester (**11**) followed by addition of an amine-derivatized Man structure (Scheme 2b).³⁷ The resulting compound **12** showed much improved solubility in water and was subsequently used for cell imaging.

Fluorescence turn-on studies

The solutions of compounds **8-12** were minimally fluorescent, but all displayed visible fluorescence after irradiation with a handheld UV lamp. Compound **8** was chosen as the model fluorogen to study the photochemical conversion. Upon irradiating compound **8** in MeOH at 350 nm for 4 h, a clean conversion of compound **8** to product **13** was observed (> 90% by ¹H NMR) (Scheme 3a). After purification by flash column chromatography, product **13** was isolated as the only fluorescent compound in 68% yield. The product was characterized by NMR and HRMS (Figs. S19-S21). To further confirm that the product was formed via the intramolecular insertion rather than hydrogen abstraction from neighboring molecules to give **14**, compound **14** was independently synthesized by reducing compound **8** by catalytic hydrogenation (Scheme 3b). In addition to the differences in NMR and IR (Figs. S23-S26), compound **14** fluoresced at a

much shorter wavelength at ~420 nm (Fig. S3) whereas product **13** emitted at 550 nm (Fig. 2c).

Scheme 3. Reactions of compound **8**: a) photo-initiated intramolecular C-H insertion; and b) reduction to aniline.



Conditions: a) Compound **8** (100 mg) in MeOH (120 mL), N₂ atmosphere, 350 nm (Rayonet photochemical reactor), 4 h, isolated yield (NMR yield); b) compound **8** (200 mg) in THF (1 mL), Pd/C (34 mg, 0.032 mmol) in MeOH (2 mL), H₂, r.t., 5 h, isolated yield.

The photo-activation of the PFAA fluorogens was monitored by UV-vis and fluorescence spectroscopy, and the results are shown in Fig. 1 (compound **8**) and Fig. S2 (compounds **9-10**). The increased absorption at 378 nm was a result of formation of product **13** (Fig. 1a), attributed to the increased conjugation in the product (Scheme 3a). The process was also accompanied by a decrease of absorption at 328 nm which is from the intact carbazole moiety (Fig. 1a). The absorption profile could be fitted to a typical first-order kinetic model, which gave a half-life (*t*_{1/2}) of approximately 12 seconds (Fig. 1b). While compound **8** showed negligible fluorescence, the emission of compound **13** at 550 nm was more than 200 times higher than for compound **8** (Fig. 1c). This demonstrates a high contrast between the on and off states of the fluorogen, a property that is critically important in imaging where fluorescence from the excited product needs to be easily distinguished from the precursor to give clear images and high signal-to-noise ratios. Moreover, the Stokes shift of fluorescent product **13** was more than 170 nm. The irradiation wavelength for compound **8** (300 nm) and the excitation wavelength for product **13** (378 nm) were well separated, which is convenient for practical operation.

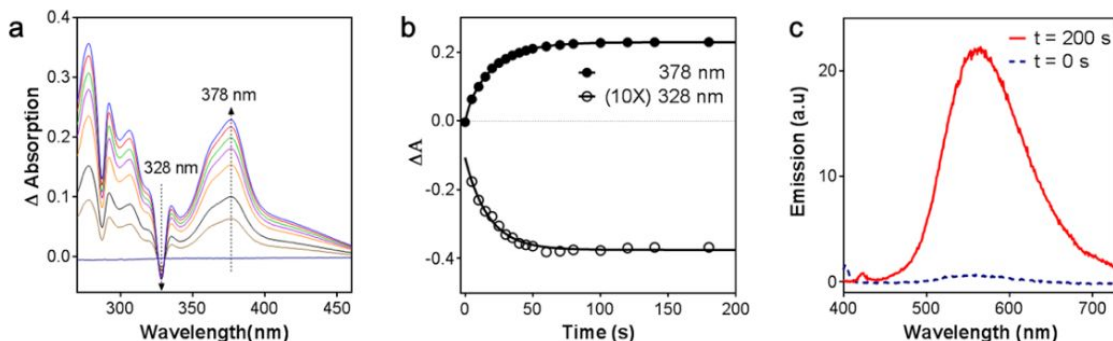


Figure 1. Characterization of the photo-activated fluorescence turn-on process of compound **8** by UV-vis and fluorescence spectroscopy. a) Absorption changes of compound **8** during photo-activation. These are difference spectra obtained by subtraction the initial spectrum without light-activation. Direction of arrows indicates increase in irradiation time. b) Changes in the absorption at 328 nm and 376 nm vs. irradiation time. Lines drawn to aid visualization. c) Fluorescence spectra before and after 350 nm irradiation for 200 s, excitation wavelength: 378 nm.

The photo-activation of compounds **8** and **12** were additionally evaluated by fluorescence microscopy. In the experiment shown in Fig. 2, both compounds were deposited on the same cover slip to keep the conditions consistent, and the right half of the sample was then irradiated at 312 nm for 30 s (Fig. 2a). The irradiated areas showed the anticipated fluorescence, yellow for compound **8** and green for compound **12**, respectively (right panel inserts), and the un-irradiated areas remained dark (left panel inserts). The fluorescence intensity of the regions after irradiation were ~ 30 and ~ 14 times higher than those before irradiation for compounds **12** and **8**, respectively (Figs. 2b and 2c), demonstrating that the photo-activation could be spatially resolved and the fluorescence turn-on was of good contrast. Additionally, the emission profiles of the fluorescence spectra after irradiation (black curves, Figs. 2b and 2c) were the same as those before irradiation (green curves). It can therefore be concluded that the two fluorogens underwent the same photon-promoted reaction despite the difference in the substitution pattern on the PFAA structure.

The photophysical and photochemical parameters of the azide-masked fluorogens, together with the previously reported perfluorophenyl azide-derivatized dihydrofuran fluorophore **1** are displayed in Table 2. Compared to compound **1**, compounds **8-10** showed shorter absorption wavelengths for the fluorogen ($\lambda_{\text{abs, azide}}$) and the product ($\lambda_{\text{abs, p}}$), but comparable conversions and quantum yields (Φ_{F} , except for **10**). The fluorescence of the irradiated product was the strongest for compound **9** and was much weaker in the case of compound **10**. The photo-conversion quantum yield (Φ_{p}) measures the probability of the azide transformation for each photon absorbed. Compared to compound **1** (0.017), compounds **8-10** displayed higher values of Φ_{p} by a factor of at least 10 (0.18-0.62). The substituent on the carbazole moiety also influenced Φ_{p} , with compound **10** (R = OMe) being the highest at 0.62. Masked fluorogens with high photo-conversion efficiency enable photoactivation at lower illumination intensity, leading to less photo-damage.³⁸ These results demonstrate that the PFAA fluorogens possess excellent photoactivatable fluorescence switch-on properties.

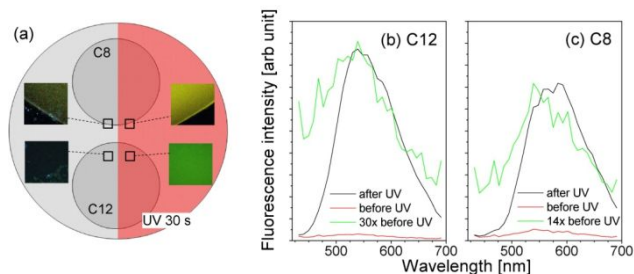


Figure 2. Characterization of the dynamic fluorescence turn-on processes of compounds **8** (C8) and **12** (C12) by confocal fluorescence microscopy. (a) Schematic of the prepared sample and lambda-mode micrographs of the four regions of interest showing the photo-activation of compounds **8** and **12**. Stock solutions of compounds **8** and **12** (10 mM in ethanol) were dropped on a glass coverslip in two separate regions (top: compound **8**, bottom: compound **12**) which were covered with smaller coverslips (shown as smaller circles) and then sealed with nail polish. The right half of the sample (pink color) was irradiated for 30 s using a UV table (Spectroline Ultraviolet Transilluminator TVC-312R/F, 312 nm). (b, c) Fluorescence spectra of compounds **12** and **8** before and after photoactivation. The green curves were the red curves amplified at 30x and 14x, respectively. A fiber-coupled LED 300 nm (Thorlabs M300F2, ca 250 mA with a spot size ca 3 mm) was used to irradiate the sample.

Cell imaging

The PFAA fluorogen was then evaluated in *in vitro* imaging using human umbilical vein endothelial (HUVEC) cells (Fig. 3). In the experiment, Man-derivatized PFAA fluorogen **12** was cultured at a concentration of 10 μM with HUVEC cells for 4 h. The cells were then irradiated by LED (300 nm), focused on the spot of the focal area of the microscope objective (Fig. 3a), and the process was monitored by confocal fluorescence microscopy. Fig. 3b is a representative merged micrograph after switching on the LED for 3 min. The temporal development of the bright-field (dashed lines) and fluorescence (solid lines) signals of four regions of interest (ROIs) are shown in Fig. 3c (LED switched on at $t = 1$ min). The fluorescence from the cells increased with the photo-activation time. This observation is consistent with the fluorescence micrographs collected at 0, 2, 4 and 6 min (Fig. 3d).

Table 2. Photophysical and photochemical parameters of the azide fluorogens.

Azide	$\lambda_{\text{abs, azide}}$ (nm) ^a { ϵ_{max} ($\text{M}^{-1} \text{cm}^{-1}$)}	$\lambda_{\text{abs, p}}$ (nm) ^b { ϵ_{max} ($\text{M}^{-1} \text{cm}^{-1}$)}	λ_{fl}^c (nm)	Yield ^d (%)	Φ_{F}^e (%)	$t_{1/2}^f$ (s)	Φ_{p}^g { λ_{p}^h }
1 ^k	407 {26,700}	463 {20,000}	578	87	0.62	85 ⁱ	0.017 ⁱ {385 nm}
8	328 {12,400}	376 {22,890}	550	80	0.51	15 ⁱ	0.18 ⁱ {350 nm}
9	345 {13,830}	378 {15,670}	538	95	0.76	10 ⁱ	0.46 ⁱ {350 nm}
10	358 {13,830}	394 {16,200}	581	90	0.11	6 ⁱ	0.62 ⁱ {350 nm}

^aPeak absorbance and molar absorptivity of azide fluorogen. ^bPeak absorbance and molar absorptivity of product. ^cPeak fluorescence emission of product. ^dBy NMR, showing the percentage of the starting azide transformed into the amine product. ^eFluorescence quantum yield of the corresponding product after photo-activation. ^fPhotoconversion half-life. ^gPhotoconversion quantum yield of azide. ^hWavelength used to photoactivate azide fluorogen. ⁱLight intensity: 1.1 mW cm^{-2} . ^jLight intensity: 0.46 mW cm^{-2} . ^kData from reference 21. Measurements for compounds **8-10** were performed in ethanol at 10 μM concentration.

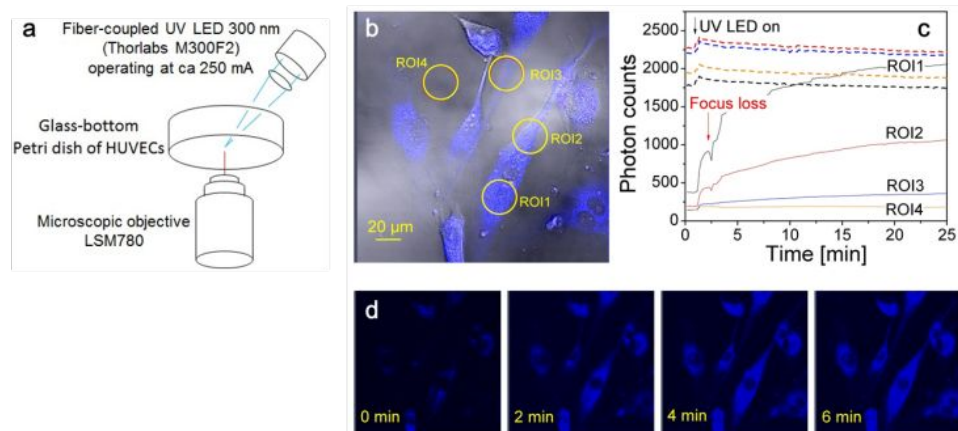


Figure 3. *In situ* photo-activation of compound **12** incubated with HUVEC cells. a) Schematic illustration of experimental setup. b) Merged bright-field and fluorescence micrograph 3 min after switching on the UV LED (Fiber-Coupled LED 300 nm, Thorlabs M300F2). Images were obtained on a confocal fluorescence microscope (Zeiss LSM780). The transmission of the radiation of 300 nm from the UV LED through the microscopic objective was very limited so the built-in laser (405 nm) was used to generate the bright-field micrographs for calibrating the fluorescence acquisition. c) Photon counts of four representative regions of interests (ROIs) on the sample. Solid lines: fluorescence signals, dashed lines: bright-field signals. d) Fluorescence micrographs at 0, 2, 4, 6 min of irradiation. Blue color is the pseudo color, showing the fluorescence channel (410–695 nm), while the bright field was generated by the built-in excitation laser of 405 nm.

Encouraged by the above results, we next tested the PFAA fluorogens for cell imaging using both compound **8** and compound **12**. Cultured HUVEC cells were incubated with each compound (10 μ M) for 4 h, after which the cells were washed with fresh growth medium, and were then subjected to photoactivation (312 nm) for 30 s. Minimal fluorescence was observed for cells incubated with **8** or **12** (Fig. 4). After photoactivation, strong fluorescence was seen and the fluorescence was distributed in the entire cell except the nucleus. This is consistent with our previous study which showed high cellular tolerance of PFAA.⁴³ After 24 h, the fluorescence remained strong across the whole cells for compound **8**, whereas compound **12** seems to be dissipated from the cells. The difference in the mode of action between compound **8** and compound **12** warrants future investigation.

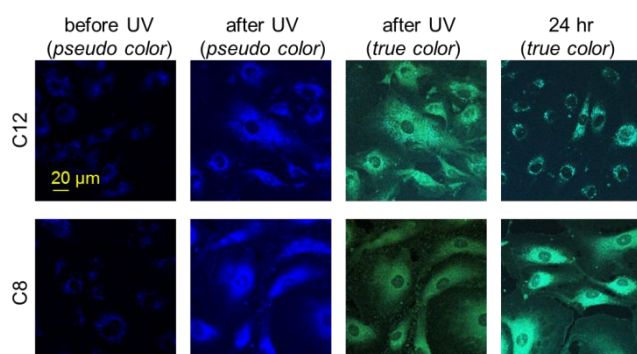


Figure 4. Fluorescence micrographs of HUVEC cells incubated with 10 μ M compound **12** (C12) or **8** (C8) for 4 h before and after UV activation. 15 μ L of the stock solution of compound **12** or **8** (1 mM in 99.5% ethanol, analytical grade) was injected into the cell culture (1.5 mL) to obtain the final concentration of 10 μ M. The ‘before UV’ images show the pseudo color of the fluorescence channel (410–695 nm). The ‘after UV’ images show both the pseudo color and the true color of the fluorescence. The ‘24 hr’ image shows the true color of the fluorescence.

To identify the location of the fluorogen, cells were co-stained with LysoTracker 633, a fluorophore that freely permeates cell membranes but is retained in acidic subcellular compartments, such as the lysosome. Fig. 5 are the confocal images showing

the locations of compound **12** and lysosome. It is clear from the merged image that compound **12** was localized in the lysosome.

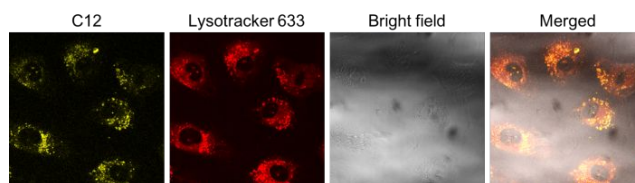


Figure 5. Fluorescence micrographs of C12-treated HUVEC cells co-stained with LysoTracker 633 (4 h) taken at different excitation. Excitation lasers: 633 nm 0.7000% and 405 nm 3.0%. Filters: 491–618 nm; LysoTracker 633: 642–695 nm. Both yellow and red are pseudo-colors.

CONCLUSIONS

In summary, we have developed azide carbazole derivatives as masked fluorogens, which undergo photo-activated fluorescence turn-on resulting from nitrene-mediated intramolecular C–H insertion. The photochemical reaction was clean, fast and highly efficient. These compounds exhibited high signal amplification and contrast. This new class of azide-masked fluorogens was efficiently prepared by nucleophilic aromatic substitution of perfluoroaryl azides with carbazole. The structure could be further derivatized or modified to introduce functional groups or ligands. The photochemical conversion is compatible with bioimaging, and the process could be conveniently monitored by fluorescence microscopy. The versatile system could find utilities in other imaging applications that require spatio-temporal controls.

EXPERIMENTAL SECTION

General methods. Reagents and solvents were used as received from Sigma Aldrich, Alfa Aesar, Fluka, and Merck. Thin-layer chromatography was conducted using TLC silica gel 60 F₂₅₄ (Merck Co.), visualized with ultraviolet light. Oil bath was used to control the reaction at high temperature. ¹H-, ¹³C- and ¹⁹F-NMR data were recorded on Bruker Ascend™ 400 or DMX 500 instruments. Chemical shifts are reported as δ values (ppm) with (residual) solvent as internal reference. All ¹³C NMR spectra were recorded as proton-decoupled data. ¹⁹F NMR signals were referenced to hexafluorobenzene ($\delta = -161.75$ in

CDCl₃ or -162.65 in DMSO-*d*₆) unless noted otherwise. High-resolution electrospray ionization (HRMS-ESI) mass spectrometry data were obtained from Proteomika tuumiklabor at the University of Tartu, Estonia, or from the Mass Spectrometry Lab at the University of Illinois at Urbana-Champaign. Infrared spectra (IR) were recorded on a ReactIR™ IC10 (Mettler Toledo Co.) for liquid samples, or a SPECTRUM 2000 (Perkin Elmer) for solid samples in the ATR mode. UV-vis absorption spectra were measured on a PerkinElmer Lambda 750 spectrophotometer with 2 nm slit width. Fluorescence spectra were recorded on the Varian Cary Eclipse Fluorescence Spectrophotometer. Quantum yields were determined using quinine sulfate in 0.1 M aq. H₂SO₄ as reference (quantum yield: 0.55). The methods for quantitative measurements of photophysical and photochemical parameters were reported in supporting information.

Methyl pentafluorobenzoate (**5**) and carbazole (**7a**) were purchased from Alfa Aesar and were used as received. Methyl 4-azido-2,3,5,6-tetrafluorobenzoate (**6**) was synthesized by following our previously reported protocol, and was characterized by comparing with the ¹⁹F and ¹H NMR data in the publication.⁴⁴ 3,6-Dibromo-9H-carbazole (**7b**) and 3,6-dimethoxy-9H-carbazole (**7c**) were synthesized following reported protocols, and the identities were confirmed by comparing with the literature ¹H and ¹³C NMR data.⁴⁵ 2-Aminoethyl α-D-mannopyranoside was synthesized following our previously reported protocol, and the identity was confirmed by comparing with the reported ¹H and ¹³C NMR data.³⁷

Methyl 4-azido-2,5-di(9H-carbazol-9-yl)-3,6-difluorobenzoate (8). To a solution of compound **6** (100 mg, 0.40 mmol) in DMSO (5 mL), carbazole (180 mg, 1.07 mmol) was added, followed by cesium carbonate (650 mg, 2.0 mmol) in portions. The mixture was heated at 50 °C until TLC showed a full conversion of the azide. Afterwards, the mixture was quenched with water (8 mL) and 1 M aq. HCl (2 mL), and further extracted with toluene (20 mL × 3 times). The combined organic phase was then washed with water (60 mL) and brine (60 mL), and dried over MgSO₄. After removal of toluene, the crude was purified by flash column chromatography (toluene/hexanes 3:2, R_f = 0.22) to give compound **8** (180 mg) as a light-yellow solid foam (86% yield). ¹H NMR (500 MHz, DMSO-*d*₆): δ_H 3.17 (s, 3H), 7.38 (m, 4H), 7.53 (m, 4H), 7.61 (t, 4H, J_{HH} = 7.3 Hz), 8.29 (t, 4H, J_{HH} = 7.3 Hz); ¹³C{¹H} NMR (101 MHz, DMSO-*d*₆): δ 52.7, 110.3, 110.5, 116.7, 116.9, 117.7, 117.9, 120.5, 120.6, 120.9, 121.0, 123.0, 123.2, 124.9, 126.3, 126.5, 140.2, 140.4, 148.7, 151.2, 152.3, 154.8, 161.1; ¹⁹F NMR (375 MHz, DMSO-*d*₆): δ -122.9 (d, 1F, J_{FF} = 13.0 Hz), -131.2 (d, 1F, J_{FF} = 13.0 Hz); HRMS-ESI FTICR analyzer: Calcd. for C₃₂H₂₀F₂N₅O₂ [M+H]⁺: 544.1585, found 544.1587; IR (ATR) see Supporting Information.

Methyl 4-azido-2-(9H-carbazol-9-yl)-3,5,6-trifluorobenzoate (8a): the mono-substituted derivative. Isolated in trace amount from the synthesis of compound **8**. ¹H NMR (500 MHz, DMSO-*d*₆): δ_H 3.19 (s, 3H), 7.23 (d, 2H, J_{HH} = 7.3 Hz), 7.32 (t, 2H, J_{HH} = 7.3 Hz), 7.44 (t, 4H, J_{HH} = 7.3 Hz), 7.23 (d, 2H, J_{HH} = 7.3 Hz). ¹⁹F NMR (375 MHz, DMSO-*d*₆): δ -132.2 (m, 1F), -140.5 (m, 1F), -143.9 (m, 1F); HRMS-ESI FTICR analyzer: Calcd. for C₂₀H₁₂F₃N₄O₂ [M+H]⁺: 397.0912, found 397.0917; IR (ATR) see Supporting Information.

Methyl 4-azido-2,5-bis(3,6-dibromo-9H-carbazol-9-yl)-3,6-difluorobenzoate (9). Synthesized following a similar protocol as for compound **8**. Light yellow solid (214 mg, 75%). R_f = 0.61 (1:1 toluene/hexanes). ¹H NMR (500 MHz, DMSO-

*d*₆): δ 3.22 (s, 3H), 7.59 (m, 4H), 7.71 (t, 4H, J_{HH} = 8.5 Hz), 8.63 (m, 4H); ¹³C{¹H} NMR (101 MHz, DMSO-*d*₆): δ 52.9, 112.5, 112.8, 113.5, 113.6, 116.3, 116.4, 117.1, 117.2, 123.9, 124.1, 129.6, 129.8, 133.1, 139.2, 139.5, 149.2, 151.2, 152.5, 154.6, 160.8; ¹⁹F NMR (375 MHz, DMSO-*d*₆): δ -122.3 (d, 1F, J_{FF} = 13.0 Hz), -131.6 (d, 1F, J_{FF} = 13.0 Hz); HRMS-ESI FTICR analyzer: Calcd. for C₃₂H₁₆Br₂F₂N₅O₂ [M+H]⁺: 855.8006, found 855.8010; IR (ATR) see Supporting Information.

Methyl 4-azido-2,5-bis(3,6-dimethoxy-9H-carbazol-9-yl)-3,6-difluorobenzoate (10). Synthesized following a similar protocol as for compound **8**. Yellow solid (133 mg, 82%). R_f = 0.25 (1:3 EtOAc/hexanes). ¹H NMR (500 MHz, DMSO-*d*₆): δ 3.19 (s, 3H), 3.91 (s, 12H), 7.10 (m, 4H), 7.45 (t, 4H, J_{HH} = 8.0 Hz), 8.60 (dd, 4H, J_{HH} = 7.3, 2.3 Hz); ¹³C{¹H} NMR (101 MHz, DMSO-*d*₆): δ 52.7, 55.66, 55.69, 103.4, 103.6, 111.2, 111.3, 115.2, 115.4, 116.7, 116.9, 118.0, 118.1, 123.7, 123.9, 124.6, 124.8, 132.7, 135.57, 135.64, 148.6, 150.6, 152.4, 154.3, 154.4, 161.3; ¹⁹F NMR (375 MHz, DMSO-*d*₆): δ -123.5 (d, 1F, J_{FF} = 13.0 Hz), -131.5 (d, 1F, J_{FF} = 13.0 Hz); HRMS-ESI FTICR analyzer: Calcd. for C₃₆H₂₈F₂N₅O₆ [M+H]⁺: 664.2008, found 664.2009; IR (ATR) see Supporting Information.

Methyl 3-(9H-carbazol-9-yl)-1,4-difluoro-5H-indolo[3,2,1-de]phenazine-2-carboxylate (13). In a 200 mL flask, compound **8** (100 mg) was dissolved in 120 mL MeOH. After the solution was purged with N₂ for 10 minutes, the flask was put under 350 nm UV inside the a Rayonet photochemical reactor. When TLC displayed full conversion (~4 h), the mixture was evaporated to give a light red solid. The crude was dissolved in chloroform, and silica gel (600 mg) was added. The crude was then purified by dry-loading column chromatography using toluene/hexanes (140:100) as eluent to give compound **13** as yellow flakes (68 mg, 68%). ¹H NMR (500 MHz, DMSO-*d*₆): δ 3.15 (s, 3H), 6.50 (d, 1H, J_{HH} = 7.5 Hz), 6.93 (t, 1H, J_{HH} = 7.5 Hz), 7.32 (m, 6H), 7.46 (m, 3H), 7.79 (t, 1H, J_{HH} = 7.4 Hz), 8.06 (d, 1H, J_{HH} = 7.8 Hz), 8.23 (d, 1H, J_{HH} = 7.8 Hz), 9.39 (br, 1H, *NH*); ¹³C{¹H} NMR (101 MHz, DMSO-*d*₆): δ 52.3, 107.1, 109.8, 111.3, 111.4, 112.2, 114.4, 114.6, 120.4, 120.5, 120.6, 121.3, 122.3, 122.9, 124.4, 124.9, 126.1, 126.3, 130.0, 130.8 (m), 131.3, 136.3, 140.3, 141.7, 143.6, 143.8, 145.8, 161.8; ¹⁹F NMR (375 MHz, DMSO-*d*₆): δ -121.8 (t, 1F, J_{FF} = 7.7 Hz), -142.6 (d, 1F, J_{FF} = 9.4 Hz); HRMS-ESI FTICR analyzer: Calcd. for C₃₂H₁₉F₂N₅O₂ [M]⁺: 515.1445, found 515.1448; IR (ATR) see Supporting Information.

Methyl 4-amino-2,5-di(9H-carbazol-9-yl)-3,6-difluorobenzoate (14). To a two-necked flask charged with Pd/C powder (34 mg, 0.032 mmol) in MeOH (2 mL) under H₂, compound **8** (200 mg) in THF (1 mL) was injected. The mixture was vigorously stirred at rt. When TLC indicated full conversion, the mixture was filtered through celite quickly and the organic phase was dried over MgSO₄. Evaporation of the organic solution gave compound **14** as a white solid (190 mg, 90% yield). ¹H NMR (500 MHz, DMSO-*d*₆): δ 3.05 (s, 3H), 6.52 (br, 2H), 7.33 (m, 4H), 7.42 (m, 4H), 7.50 (m, 4H), 8.27 (t, 4H, J_{HH} = 7.7 Hz); ¹³C{¹H} NMR (101 MHz, DMSO-*d*₆): δ 51.7, 104.1, 104.2, 109.2, 109.3, 110.0, 110.1, 120.3, 120.4, 120.5, 122.9, 123.5, 123.6, 126.16, 126.19, 140.2, 140.6, 140.9 (m), 142.7, 144.6, 154.5, 156.5, 162.0; ¹⁹F NMR (375 MHz, DMSO-*d*₆): δ -122.7 (d, 1F, J_{FF} = 11.4 Hz), -140.9 (d, 1F, J_{FF} = 9.4 Hz); HRMS-ESI FTICR analyzer: Calcd. for C₃₂H₂₂F₂N₅O₂ [M+H]⁺: 518.1680, found 518.1689; IR (ATR) see Supporting Information.

2,5-Dioxopyrrolidin-1-yl 4-azido-2,5-di(9H-carbazol-9-yl)-3,6-difluorobenzoate (11). To a flask charged with compound **8** (270 mg, 0.5 mmol) in MeOH (40 mL) and THF

(12 mL), aqueous sodium hydroxide solution (20%, w/w; 10 mL) and water (5 mL) were added. The mixture was then stirred at rt. When TLC showed full conversion (~5 h), the mixture was acidified with 1 M aq. HCl and extracted with CHCl₃ (3 x 60 mL). The solvent was evaporated under reduced pressure to give the crude intermediate. The crude intermediate was then dissolved in DCM (30 mL) containing *N*-hydroxysuccinimide (65 mg, 0.56 mmol) and EDAC (164 mg, 0.86 mmol), and the mixture were stirred at rt. When TLC indicated full conversion (~48 h), the mixture was diluted with water (50 mL) and extracted twice with DCM (2 x 30 mL). The combined organic phase was washed with water, dried over MgSO₄, and evaporated under reduced pressure. The crude was purified by flash column chromatography using EtOAc/hexanes (1:3, R_f = 0.13) as eluent to give compound **11** as a pale yellow solid (219 mg, 70%). ¹H NMR (500 MHz, DMSO-*d*₆): δ 3.59 (s, 4H), 7.35 (t, 2H, J_{HH} = 7.3 Hz), 7.41 (t, 2H, J_{HH} = 7.3 Hz), 7.49 (t, 2H, J_{HH} = 7.3 Hz), 7.56 (t, 2H, J_{HH} = 7.3 Hz), 7.64 (d, 2H, J_{HH} = 7.7 Hz), 7.70 (d, 2H, J_{HH} = 7.7 Hz), 8.23 (d, 2H, J_{HH} = 7.7 Hz), 8.31 (d, 2H, J_{HH} = 7.7 Hz); ¹³C {H} NMR (126 MHz, DMSO-*d*₆): δ 25.3, 110.3, 110.6, 111.2, 111.4, 120.4, 120.7, 120.8, 121.1, 123.1, 123.2, 126.4, 126.6, 135.8, 140.2, 140.5, 149.6, 151.6, 154.0, 156.1, 156.9, 169.1; ¹⁹F NMR (375 MHz, DMSO-*d*₆): δ -116.3 (d, 1F, J_{FF} = 12.6 Hz), -130.3 (d, 1F, J_{FF} = 12.6 Hz); HRMS-ESI FTICR analyzer: Calcd. for C₃₅H₂₁F₂N₆O₄ [M+H]⁺: 627.1592, found 627.1596; IR (ATR) see Supporting Information.

4-Azido-2,5-di(9H-carbazol-9-yl)-3,6-difluoro-N-(2-((2S,3S,4S,5S,6R)-3,4,5-trihydroxy-6-(hydroxymethyl)tetrahydro-2H-pyran-2-yl)oxy)ethyl)benzamide (12). To a solution of compound **11** (110 mg, 0.18 mmol) in DMF (3 mL) in the dark, 2-aminoethyl α-D-mannopyranoside (51 mg, 0.23 mmol) was added. The mixture was stirred at rt for 24 h. The solvent was directly evaporated *in vacuo* at rt. Afterwards, the crude was purified by flash column chromatography (DCM/MeOH 11:1, R_f = 0.1) to give compound **11** (77 mg, 55%) as a pink solid. ¹H NMR (400 MHz, CD₃CN): δ 2.82 (m, 2H), 2.94 (m, 1H), 3.14 (m, 4H), 3.20 (m, 1H), 3.30 (m, 1H), 3.45 (m, 2H), 3.55 (m, 3H), 4.38 (s, 1H), 7.25 (s, 1H, NH), 7.40 (m, 4H), 7.50 (m, 4H), 7.54 (m, 4H), 8.20 (d, 2H, J_{HH} = 7.6 Hz), 8.24 (t, 2H, J_{HH} = 7.6 Hz); ¹³C {H} NMR (101 MHz, CD₃CN): δ 25.7, 39.5, 62.2, 66.2, 68.2, 70.9, 71.8, 73.2, 100.4, 110.7, 110.9, 111.0, 120.9, 121.2, 121.7, 123.7, 123.9, 124.0, 124.1, 126.9, 127.2 (m), 131.6 (m), 141.1, 141.4, 141.5, 149.6 (m), 152.2 (m), 154.7 (m), 160.26; ¹⁹F NMR (375 MHz, CD₃CN): δ -125.1 (d, 1F, J_{FF} = 14.0 Hz), -133.5 (d, 1F, J_{FF} = 14.0 Hz); HRMS-ESI FTICR analyzer: Calcd. for C₃₉H₃₂F₂N₉O₇Na [M+Na]⁺: 799.2290, found 799.2294; IR (ATR) see Supporting Information.

Quantitative measurements of photophysical and photochemical parameters. Measurements were carried out using reported protocols,^{17-18, 21} at low concentrations to avoid complications with aggregate formation. Molar absorption coefficients were measured from serial dilutions with known concentrations. Samples were prepared in MeOH unless noted otherwise. A hand-held UV lamp (365 nm) or a Rayonet photochemical reactor (350 nm) were used as light sources. The intensity of the light was determined by a UV-light meter (Sentry Optronics Corp.) before experiments. The sample solutions were freshly prepared and quartz cuvettes were used as reaction vessels. The solutions were not purged with N₂ before measurement. The photo-conversion was monitored by measuring changes in absorbance of the reactant and photoproduct of interest in MeOH over time (Fig. S1). The

quantum yield of the photoconversion (Φ_p) was estimated by the following equation:²¹

$$\Phi_p = \frac{R_p}{R_{abs}} = \frac{1}{\tau_p I_\lambda \sigma_\lambda \left(\frac{\lambda}{hc}\right)}$$

where τ_p is the exponential time constant from fitting the decaying absorption (Fig. S2b), and equals t_{1/2}/ln2; I_λ is the irradiation intensity, measured to be 0.46 mW cm⁻² in all cases; σ_λ is the absorption cross-section; λ is the excitation wavelength; *h* is Planck's constant; *c* is the speed of light.

Cell imaging. Human umbilical vein endothelial cells (HUVEC) were purchased from Lonza and cultured in EGM-2 medium (EGM-2MV Basal Medium+EGM-2MV SingleQuots) complemented with 1% penicillin/streptomycin/glutamine, and 0.1% amphotericin B. Cells of passage 2-5 were used in the experiments. Compounds incubated with HUVEC cells were studied by confocal and bright-field microscopy. HUVEC cells cultured in glass-bottom dishes were placed directly on the microscope sample-stage incubator, and imaged using Zeiss LSM 780 confocal microscope (Carl Zeiss, Jena, Germany) with either C-Apochromat 40x/1.20 W Korr FCS M27 objective using multiple channels, z-stack, and lambda scan modes. The excitation wavelength was 405 nm. TIFF micrographs were exported from ZEN original image files, using software ZEN 2012 (Zeiss, Germany) without compression, and analyzed offline using MATLAB. UV irradiations were done on a UV table: Spectroline ultraviolet transilluminator TVC-312R/F (312 nm), or UV LED: Fiber-Coupled LED 300 nm (Thorlabs M300F2) at ca 250 mA. Cell imaging studies were repeated at least twice for each set of experiments.

ASSOCIATED CONTENT

Supporting Information.

The synthetic scheme of 2-aminoethyl α-D-mannopyranoside, UV-*vis* spectra of perfluoroaryl compounds and carbazole, photochemical reactions of compounds **9** and **10** monitored by UV-*vis* and fluorescence spectroscopy, fluorescent properties of compound **14**, and NMR spectra of the synthesized compounds. This material is available free of charge via the Internet at <http://pubs.acs.org>.

AUTHOR INFORMATION

Corresponding Author

*Email: shengxie@hnu.edu.cn (S.X.).

*Email: olof_ramstrom@uml.edu (O.R.).

*Email: mingdi_yan@uml.edu (M.Y.).

ACKNOWLEDGMENT

We thank Prof. Ying Fu for help with the fluorescence imaging. This work was supported in part by NIH (R15GM128164 to M.Y.).

REFERENCES

- (1) Patterson, G. H.; Lippincott-Schwartz, J. A photoactivatable GFP for selective photolabeling of proteins and cells. *Science* **2002**, *297*, 1873.
- (2) Gu, X.; Zhao, E.; Lam, J. W.; Peng, Q.; Xie, Y.; Zhang, Y.; Wong, K. S.; Sung, H. H.; Williams, I. D.; Tang, B. Z. Mitochondrion-Specific Live-Cell Bioprobe Operated in a Fluorescence Turn-On Manner and a Well-Designed Photoactivatable Mechanism. *Adv. Mater.* **2015**, *27*, 7093.

- (3) Politz, J. C. Use of caged fluorochromes to track macromolecular movement in living cells. *Trends Cell Biol.* **1999**, *9*, 284.
- (4) Fernandez-Suarez, M.; Ting, A. Y. Fluorescent probes for super-resolution imaging in living cells. *Nat. Rev. Mol. Cell Biol.* **2008**, *9*, 929.
- (5) Raymo, F. M. Photoactivatable Synthetic Dyes for Fluorescence Imaging at the Nanoscale. *J. Phys. Chem. Lett.* **2012**, *3*, 2379.
- (6) Shao, Q.; Xing, B. Photoactive molecules for applications in molecular imaging and cell biology. *Chem. Soc. Rev.* **2010**, *39*, 2835.
- (7) Betzig, E.; Patterson, G. H.; Sougrat, R.; Lindwasser, O. W.; Olenych, S.; Bonifacino, J. S.; Davidson, M. W.; Lippincott-Schwartz, J.; Hess, H. F. Imaging intracellular fluorescent proteins at nanometer resolution. *Science* **2006**, *313*, 1642.
- (8) Li, W. H.; Zheng, G. Photoactivatable fluorophores and techniques for biological imaging applications. *Photochem. Photobiol. Sci.* **2012**, *11*, 460.
- (9) Lukyanov, K. A.; Chudakov, D. M.; Lukyanov, S.; Verkhusha, V. V. Innovation: Photoactivatable fluorescent proteins. *Nat. Rev. Mol. Cell Biol.* **2005**, *6*, 885.
- (10) Raymo, F. M. Photoactivatable synthetic fluorophores. *Phys. Chem. Chem. Phys.* **2013**, *15*, 14840.
- (11) Klan, P.; Solomek, T.; Bochet, C. G.; Blanc, A.; Givens, R.; Rubina, M.; Popik, V.; Kostikov, A.; Wirz, J. Photoremovable protecting groups in chemistry and biology: reaction mechanisms and efficacy. *Chem. Rev.* **2013**, *113*, 119.
- (12) Bao, C.; Zhu, L.; Lin, Q.; Tian, H. Building biomedical materials using photochemical bond cleavage. *Adv. Mater.* **2015**, *27*, 1647.
- (13) Yu, Z.; Ho, L. Y.; Lin, Q. Rapid, photoactivatable turn-on fluorescent probes based on an intramolecular photoclick reaction. *J. Am. Chem. Soc.* **2011**, *133*, 11912.
- (14) Tran, M. N.; Chenoweth, D. M. Photoelectrocyclization as an activation mechanism for organelle-specific live-cell imaging probes. *Angew. Chem. Int. Ed.* **2015**, *54*, 6442.
- (15) Gu, X.; Zhao, E.; Zhao, T.; Kang, M.; Gui, C.; Lam, J. W.; Du, S.; Loy, M. M.; Tang, B. Z. A Mitochondrion-Specific Photoactivatable Fluorescence Turn-On AIE-Based Bioprobe for Localization Super-Resolution Microscopy. *Adv. Mater.* **2016**, *28*, 5064.
- (16) Gao, M.; Su, H. F.; Lin, Y. H.; Ling, X.; Li, S. W.; Qin, A. J.; Tang, B. Z. Photoactivatable aggregation-induced emission probes for lipid droplets-specific live cell imaging. *Chem. Sci.* **2017**, *8*, 1763.
- (17) Lord, S. J.; Conley, N. R.; Lee, H. L.; Nishimura, S. Y.; Pomerantz, A. K.; Willets, K. A.; Lu, Z.; Wang, H.; Liu, N.; Samuel, R.; Weber, R.; Semyonov, A.; He, M.; Twieg, R. J.; Moerner, W. E. DCDHF fluorophores for single-molecule imaging in cells. *Chemphyschem* **2009**, *10*, 55.
- (18) Lord, S. J.; Conley, N. R.; Lee, H. L.; Samuel, R.; Liu, N.; Twieg, R. J.; Moerner, W. E. A photoactivatable push-pull fluorophore for single-molecule imaging in live cells. *J. Am. Chem. Soc.* **2008**, *130*, 9204.
- (19) Lee, H. L.; Lord, S. J.; Iwanaga, S.; Zhan, K.; Xie, H.; Williams, J. C.; Wang, H.; Bowman, G. R.; Goley, E. D.; Shapiro, L.; Twieg, R. J.; Rao, J.; Moerner, W. E. Superresolution imaging of targeted proteins in fixed and living cells using photoactivatable organic fluorophores. *J. Am. Chem. Soc.* **2010**, *132*, 15099.
- (20) Pavani, S. R.; Thompson, M. A.; Biteen, J. S.; Lord, S. J.; Liu, N.; Twieg, R. J.; Piestun, R.; Moerner, W. E. Three-dimensional, single-molecule fluorescence imaging beyond the diffraction limit by using a double-helix point spread function. *Proc. Natl. Acad. Sci. U S A* **2009**, *106*, 2995.
- (21) Lord, S. J.; Lee, H. L.; Samuel, R.; Weber, R.; Liu, N.; Conley, N. R.; Thompson, M. A.; Twieg, R. J.; Moerner, W. E. Azido push-pull fluorogens photoactivate to produce bright fluorescent labels. *J. Phys. Chem. B* **2010**, *114*, 14157.
- (22) Ankenbruck, N.; Courtney, T.; Naro, Y.; Deiters, A. Optochemical Control of Biological Processes in Cells and Animals. *Angew. Chem. Int. Ed.* **2018**, *57*, 2768.
- (23) Lin, V. S.; Lippert, A. R.; Chang, C. J. Azide-based fluorescent probes: imaging hydrogen sulfide in living systems. *Methods Enzymol.* **2015**, *554*, 63.
- (24) Shieh, P.; Dien, V. T.; Beahm, B. J.; Castellano, J. M.; Wyss-Coray, T.; Bertozzi, C. R. CalFluors: A Universal Motif for Fluorogenic Azide Probes across the Visible Spectrum. *J. Am. Chem. Soc.* **2015**, *137*, 7145.
- (25) Gritsan, N. P.; Platz, M. S. Kinetics, spectroscopy, and computational chemistry of aryl nitrenes. *Chem. Rev.* **2006**, *106*, 3844.
- (26) Budyka, M. F. Photodissociation of Aromatic Azides. *Uspekhi Khimii* **2008**, *77*, 757.
- (27) Brase, S.; Gil, C.; Knepper, K.; Zimmermann, V. Organic azides: an exploding diversity of a unique class of compounds. *Angew. Chem. Int. Ed.* **2005**, *44*, 5188.
- (28) Murata, S.; Sugawara, T.; Iwamura, H. Reactivities of Rotameric Ap and Sp-3,5-Dimethyl-2-(9-Fluorenyl)Phenyl Nitrenes. *J. Am. Chem. Soc.* **1985**, *107*, 6317.
- (29) Borden, W. T.; Gritsan, N. P.; Hadad, C. M.; Karney, W. L.; Kemnitz, C. R.; Platz, M. S. The interplay of theory and experiment in the study of phenyl nitrene. *Acc. Chem. Res.* **2000**, *33*, 765.
- (30) Liu, L. H.; Yan, M. Perfluorophenyl azides: new applications in surface functionalization and nanomaterial synthesis. *Acc. Chem. Res.* **2010**, *43*, 1434.
- (31) Park, J.; Yan, M. Covalent functionalization of graphene with reactive intermediates. *Acc. Chem. Res.* **2013**, *46*, 181.
- (32) Bordwell, F. G.; Hughes, D. L. Nucleophilic aromatic substitution reactions with carbanions and nitrenes in dimethyl sulfoxide solution. *J. Am. Chem. Soc.* **1986**, *108*, 5991.
- (33) Crawford, L. A.; Ieva, M.; McNab, H.; Parsons, S. Structural studies of some push-pull N-arylbenzazoles. *Dalton Trans.* **2010**, *39*, 7147.
- (34) Biemans, H. A.; Zhang, C.; Smith, P.; Kooijman, H.; Smeets, W. J.; Spek, A. L.; Meijer, E. W. Hexapyrrolylbenzene and Octapyrrolylnaphthalene. *J. Org. Chem.* **1996**, *61*, 9012.
- (35) Nenri, R. N.; Yeager, W. H. Reaction of diazole anions with hexafluorobenzene: an unexpectedly facile entry into hexa (diazol-1-yl)-benzenes. *Heterocycles* **1993**, *35*, 415.
- (36) Amii, H.; Uneyama, K. C-F bond activation in organic synthesis. *Chem. Rev.* **2009**, *109*, 2119.
- (37) Deng, L.; Norberg, O.; Uppalapati, S.; Yan, M.; Ramström, O. Stereoselective synthesis of light-activatable perfluorophenylazide-conjugated carbohydrates for glycoarray fabrication and evaluation of structural effects on protein binding by SPR imaging. *Org. Biomol. Chem.* **2011**, *9*, 3188.
- (38) Lord, S. J.; Lee, H. L.; Moerner, W. E. Single-molecule spectroscopy and imaging of biomolecules in living cells. *Anal. Chem.* **2010**, *82*, 2192.
- (39) Groger, M.; Holthöner, W.; Maurer, D.; Lechleitner, S.; Wolff, K.; Mayr, B. B.; Lubitz, W.; Petzelbauer, P. Dermal microvascular endothelial cells express the 180-kDa macrophage mannose receptor in situ and in vitro. *J. Immunol.* **2000**, *165*, 5428.
- (40) Sheikh, H.; Yarwood, H.; Ashworth, A.; Isacke, M. C. Endo180, an endocytic recycling glycoprotein related to the macrophage mannose receptor is expressed on fibroblasts, endothelial cells and macrophages and functions as a lectin receptor. *J. Cell Sci.* **2000**, *113*, 1021.
- (41) van den Eijnden, M. M.; Saris, J. J.; de Bruin, R. J.; de Wit, E.; Sluiter, W.; Reudelhuber, T. L.; Schalekamp, M. A.; Derkx, F. H.; Danser, A. H. Prorenin accumulation and activation in human endothelial cells: importance of mannose 6-phosphate receptors. *Arterioscler. Thromb. Vasc. Biol.* **2001**, *21*, 911.
- (42) Sharma, V.; Freeze, H. H. Mannose efflux from the cells: a potential source of mannose in blood. *J. Biol. Chem.* **2011**, *286*, 10193.
- (43) Sundhoro, M.; Jeon, S.; Park, J.; Ramström, O.; Yan, M. Perfluoroaryl Azide-Staudinger Reaction: A Fast and Bioorthogonal Reaction. *Angew. Chem. Int. Ed.* **2017**, *56*, 12117.
- (44) Xie, S.; Lopez, S. A.; Ramström, O.; Yan, M.; Houk, K. N. 1,3-Dipolar cycloaddition reactivities of perfluorinated aryl azides with enamines and strained dipolarophiles. *J. Am. Chem. Soc.* **2015**, *137*, 2958.
- (45) Louillat, M. L.; Patureau, F. W. Towards polynuclear Ru-Cu catalytic dehydrogenative C-N bond formation, one the reactivity of carbazoles. *Org. Lett.* **2013**, *15*, 164.

SYNOPSIS TOC

